Polymer Microstructures Fabricated via Laser Ablation Used for Multianalyte Protein Microassay

ARTICLE *in* LANGMUIR · NOVEMBER 2002

Impact Factor: 4.46 · DOI: 10.1021/la0260178

Polymer Microstructures Fabricated via Laser Ablation Used for Multianalyte Protein Microassay

Elena P. Ivanova,* Jonathan P. Wright, Duy Pham, Luisa Filipponi, Andrea Viezzoli, and Dan V. Nicolau*

Industrial Research Institute Swinburne, Swinburne University of Technology, PO Box 218, Hawthorn, Vic 3122, Australia

Received May 31, 2002. In Final Form: August 28, 2002

This paper describes a novel technique for the fabrication of a multianalyte protein microassay on the basis of the creation of microwells that locally enhance the adsorption of proteins. The microwells are fabricated via a localized laser ablation of a protein-blocked thin gold layer (∼50 nm) deposited on a poly(methyl methacrylate) film. The microablation of gold induces local chemical and physical changes in the top surface of the polymer as well as a higher specific surface, which cooperate to achieve a higher and more reproducible surface concentration of proteins in microwells. The fabrication platform consists of a computer-controlled laser ablation system, comprising a research-grade inverted optical microscope, a pulsed nitrogen laser emitting at 337 nm, a programmable XYZ stage, and a picoliter pipet mounted on the XYZ stage. The microwells with diameters of 5−20 μm, 1−5 μm, and submicron widths are readily achieved by focusing through a 20× dry objective, a 40× dry objective, or a 100× oil immersion lens, respectively. One variant of the method uses a sequence of local ablation and "flood" coverage with protein solution. The second variant uses the microablation of the whole microassay followed by the "spatially addressable" deposition of different protein solution with a picoliter pipet mounted on the same fabrication platform. The analytical performance of the device required only a 2−7 μL volume of sample and a single dilution step. The results indicate that antibody arrays can be used to identify different proteins, yielding results within a few minutes of sample addition with acceptable assay repeatability. It was observed that the microassays comprising line-shaped microstructures offer a higher reproducibility as well as offering the opportunity to encode the information (e.g. type of antibody, concentration) through a combination of vertical lines in a "bar code", "informationally addressable" mode and not in a 2D, spatially addressable mode like in the classical microarrays.

Introduction

Antibody-based microarrays are thought to be only the first-generation of protein-based microdevices, which are to become versatile and powerful tools for various molecular and cellular analyses including clinical diagnostics and the complete protein complement of the genome.[1−3] Protein arrays are currently under intensive exploration, but many critical aspects of their fabrication (e.g. protein−surface interaction) and functions (protein−protein interaction) are grossly underestimated when an analogy with DNA arrays is done.[4] Microarrays offer an attractive alternative to the existing biosensing or assays systems allowing rapid, moderate cost, and quantitative protein detection.[5−8] Most technologies for the fabrication of protein chips have to ensure the confinement of different protein molecules in localized areas, flat, 2D, or profiled, "2D+" microareas. Among the technologies available for the fabrication of protein chips one can mention (i) spotted-array-based methods,[9,10] (ii) soft lithography,[11,12] (iii) photolithography,[13−16] (iv) scanning probe lithography,[17] (v) laser or ion-beam ablation,[18−19] and (vi) microfabrication of profiled features for e.g. microfluidic devices.[20−24] These methods have been listed, not comprehensively, in the order of their "3D-ness", that is, starting with protein features that are elevated a few tens of nanometers above the surface (methods i−iii), to quasi-flat features (methods

* To whom correspondence should be addressed. E-mail: dnicolau@swin.edu.au (D.V.N); eivanova@swin.edu.au (E.P.I).

(1) Anderson, N. L.; Matheson, A. D.; Stiner, S. *Curr. Opin. Biotechnol.* **2000**, *11*, 408−412.
(2) Legrain, P.; Jestin, J. L.; Schachter, V. *Curr. Opin. Biotechnol.* **2000**, *11*, 402−407.
(3) Haight, R.; Hayden, M.; Longo, P.; Neary, C.; Wagner, A. *J. Vac. Sci. Technol.* **1999**, *B17* (6), 3137−3140.
(4) Kodadek, T. *Chem. Biol.* **2001**, *8*, 105−115.
(5) Rabbany, S. Y.; Donner, B. L.; Ligler, F. S. *Crit. Rev. Biomed. Eng.* **1994**, *22*, 307−346.
(6) Rowe-Taitt, C. A.; Golden, J. P.; Feldstein, M. J.; Cras, J. J.; Hoffman, K. E.; Ligler, F. S. *Biosens. Bioelectron.* **2000**, *14*, 785−794.
(7) Sapsford, K. E.; Charles, P. T.; Patterson, C. H., Jr.; Ligler, F. S. *Anal. Biochem.* **2002**, *74*, 1061−1068.
(8) Dodson, J. M.; Feldstein, M. J.; Leatzow, D. M.; Flack, L. K.; Golden, J. P.; Ligler, F. S. *Anal. Chem.* **2001**, *73*, 3776−3780.
(9) De Wildt, R. M.; Mundy, C. R.; Gorick, B. D.; Tomlinson, I. M. *Nat. Biotechnol.* **2000**, *18*, 989−994.
(10) Walter, G.; Bussow, K.; Cahill, D.; Lueking, A.; Lehrach, H. *Curr. Opin. Microbiol.* **2000**, *3*, 298−302.
(11) Zhao, X. M.; Xia, Y. N.; Whitesides, G. M. *J. Mater. Chem.* **1997**, *7*, 1067−1074.
(12) Bernard, A.; Delamarche, E.; Schmid, H.; Michel, B.; Bosshard, H. R.; Biebuyck, H. *Langmuir* **1998**, *14*, 2225−2229.
(13) Fodor, S. P. A.; Read, J. L.; Pirrung, M. C.; Stryer, L.; Lu, A. T.; Solas, D. *Science* **1991**, *251*, 767−773.
(14) Ligler, F. S.; Bhatia, S.; Schriver-Lake, L. C.; Georger, J.; Calvert, J.; Dulcey, C. U.S. Patent 5391463, 1995.
(15) Nicolau, D. V.; Taguchi, T.; Taniguchi, H.; Yoshikawa, S. *Langmuir* **1998**, *14*, 1927−1936.
(16) Nicolau, D. V.; Taguchi, T.; Taniguchi, H.; Yoshikawa, S. *Langmuir* **1999**, *15*, 3845−3851.
(17) Wadu-Mesthrige, K.; Xu, S.; Amro, N. A.; Liu, G. *Langmuir* **1999**, *15*, 8580−8583.
(18) Schwarz, A.; Rossier, J. S.; Roulet, E.; Mermod, N.; Roberts, V. A.; Girault, R. H. *Langmuir* **1998**, *14*, 5526−5531.
(19) Brizzolara, R. A. U.S. Patent 5858801, 1999.
(20) Wang, C.; Oleschuk, R.; Ouchen, F.; Li, J.; Thibault, P.; Harrison, D. J. *Rapid Commun. Mass Spectrosc.* **2000**, *14*, 1377−1383.
(21) Sundberg, S. A. *Curr. Opin. Biotechnol.* **2000**, *11*, 47−53.
(22) Nicolau, D. V.; Cross, R. *Biosens. Bioelectron.* **2000**, *15*, 85−91.
(23) McDonald, J. C.; Metallo, S. J.; Whitesides, G. M. *Anal. Chem.* **2001**, *73*, 5645−5650.
(24) Ismagilov, R. F.; Ng, J. M.; Kenis, P. J.; Whitesides, G. M. *Anal. Chem.* **2001**, *73*, 5207−5213.

10.1021/la0260178 CCC: $22.00
Published on Web 10/24/2002

iv and v), and ending with protein features that are placed on the bottom of etched or developed microfeatures (methods v and vi). While some types of biodevices dictate a particular design of the biodevices (e.g. microfluidics devices will ask for profiled channels), others do not (e.g. microarrays would have normally a flat surface). The profiled features have the advantage of minimization of interspot contamination and the drawback of more difficult access of the recognition biomolecule (e.g. antigen for antibody microarray) in a microconfined area, but an optimal shallow profile feature would take advantage of the benefit of the former and mitigate the latter.

Among the enabling technologies for the above biomolecule micropatterning methods, laser beams are capable, depending on the exposure energy and the sensitivity or adsorbance of the exposed material, to enable both photolithography and photoassisted etching. Also, focused laser beams can solve, in principle, a critical fabrication and operating problem of the protein chips better than most other alternative methods, i.e., the controlled and confined variation of the surface properties of the microareas where different proteins are deposited on.

In contrast to the simpler DNA molecules, proteins present extremely various molecular surfaces (e.g.: hydrophilic or hydrophobic; acidic or basic; neutral or charged) that interact with the surface via electrostatic forces, hydrogen-bonding, van der Waals, or hydrophobic interactions. This variety of molecular surface−biochip surface interactions can lead to large variations in protein surface concentrations as well as possibly important changing of the protein bioactivity and its denaturation. From here, different processes, in particular biomolecule immobilization on surfaces, have to be developed for protein−protein, enzyme−substrate, protein−DNA, protein−oligosaccharides, or protein−drug assay.[25] One logical approach would require to precisely tailor the surface properties to reach the same biomolecule concentration and bioactivity throughout the devices. However, this approach will not only require a very accurate control of the surface properties at the micro or nanometer level but also a priori knowledge regarding the nature of the deposited proteins and their interaction with surfaces, which is an extremely complex matter. An easier approach would be to "combinatorialize" the surface properties of all microareas that hold biomolecules.

Along this line of thinking, this work reports on the fabrication via laser ablation of shallow-profiled microstructures with surface properties of the microwells tailored to accommodate an universal adsorption of proteins.

Results and Discussion

Fabrication of Microstructures in Au-Deposited PMMA Films. Two potentially important surface-related problems of the protein chips technology are (i) the possible difference between the surface concentrations of different proteins on the same surface and (ii) the possible surface-induced denaturation of the structure and subsequently the change of the bioactivity of the adsorbed biomolecules.[26] The "combinatorialization" of the properties of the surface within a microarea would allow the probing of the "variable-space" of protein−surface interaction and therefore allow the comparison between, for example, the maximum adsorptions of different proteins in different spots.

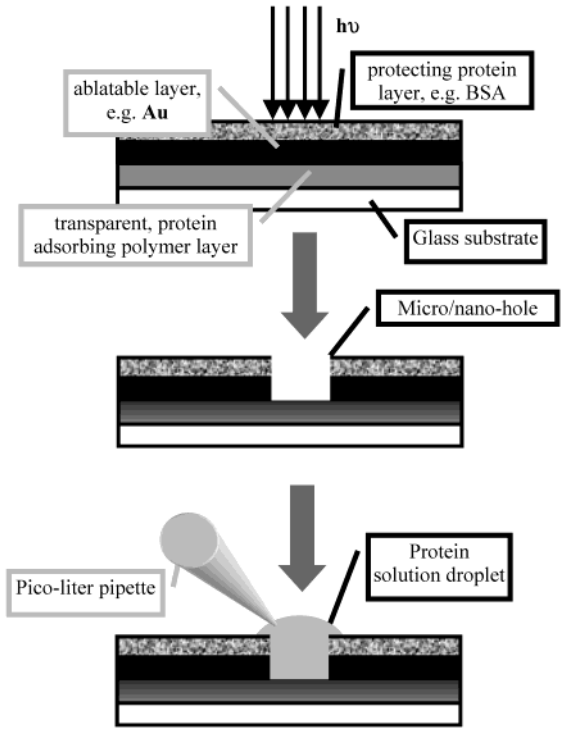

Figure 1. Procedure for direct patterning of fluorescently labeled proteins on laser-fabricated polymer surfaces.

Another, cost-related issue is the preference for the least amount possible of biomolecules used for the fabrication and operation of the microassay. While the classical microarray technology uses flat surfaces, with inherent spread of the small volume of the analyte solution in the deposited droplet, a profiled microfabricated location in which the droplet is deposited would be a more efficient solution. However, the depth of the profiled feature has to be minimized to allow a free diffusion of the analyte in the microfabricated well.

Among the many procedures for microfabrication, microablation has the advantage of a stepwise process without the involvement of fluids such as in microlithography. In principle, there are few possibilities to fabricate the microwells, all with advantages and drawbacks. First, the ablation of a protein-blocked single layer of a polymer,[18−19] preferably designed to promote protein adsorption without surface-induced denaturation, is the simplest choice. However, this approach needs to use either more expensive laser ablation tools operating in deep-UV (e.g. 248 nm) and nonfluorescent polymers (e.g. PMMA) or the use of more convenient (e.g. near-UV) lasers and polymers that absorb in that region but which are likely to interfere with the detection through background fluorescence. Second, a bilayer structure with an ablatable layer on the bottom and a protein-adsorbing, sacrificial layer on top seems an attractive option. However, our experiments (data not shown) proved that the ablated material (e.g. Au) cannot be efficiently released during the ablation through the top polymeric layer, leading to the frequent peel-off of large areas of the bilayer structure. A third possibility is to deposit a very thin ablatable layer on top of a protein-adsorbing, transparent to laser wavelength, nonablatable polymeric layer. This technological avenue raises the issue of the fate of the physics and chemistry of the top surface of the bottom layer, which is exposed to large amounts of energy during the ablation of the top layer. The logical approach would be to tune the ablation in manner that will preserve the bottom layer, but there is only a remote possibility that this can be

(25) Templin, M. F.; Stoll, D.; Schrenk, M.; Traub, P. C.; Vohringer, C. F.; Joos, T. O. *Trends Biotechnol.* **2002**, *20*, 160−166.
(26) Andrade, J. D.; Hlady, V. *J. Biomater. Sci., Polym. Ed.* **1991**, *2*, 161−72.

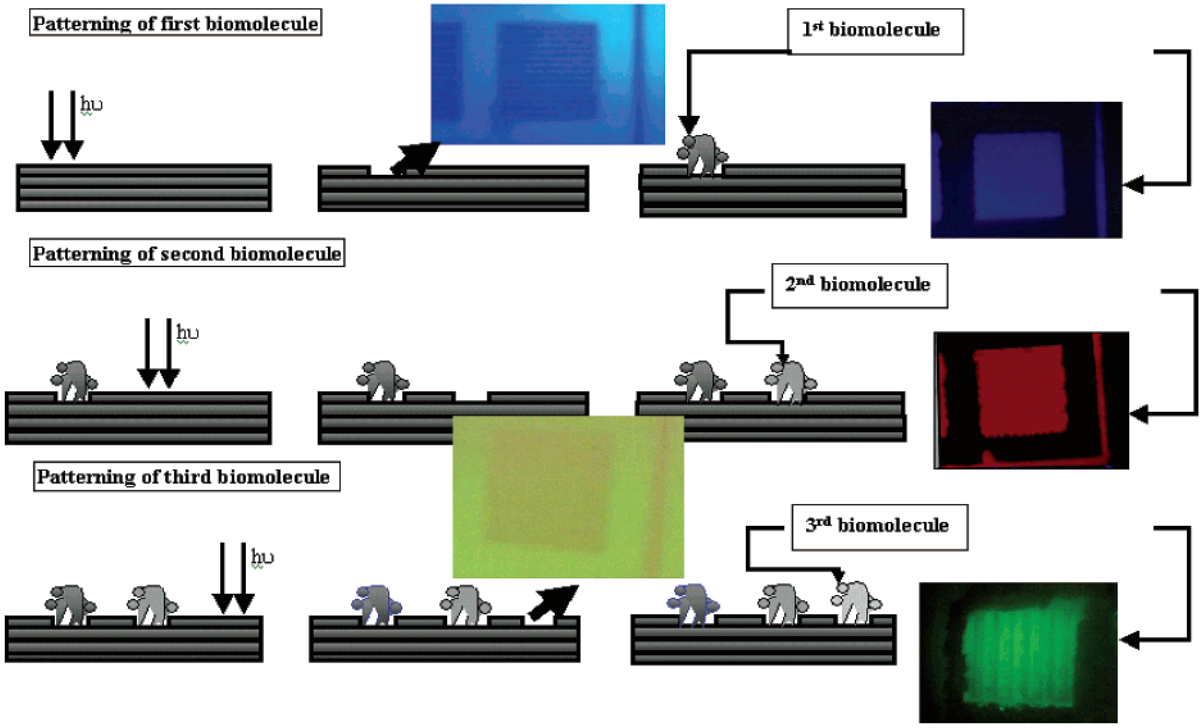

Figure 2. Process flow for the fabrication of a microablated microarray, with fluorescent images before (middle top and middle bottom) and after antibody deposition (right). The ablated microwells are 100 × 100 μm.

achieved. A similar problem arose in semiconductor lithography when lasers have been used to ablate metal defects on the surface of deep-UV masks without damaging the bottom quartz layer. It was found that only femtosecond lasers are quick enough to ablate the metal without damaging the glass.[3] However, apart from not ensuring the integrity of the bottom layer, as glass is much more thermoresistant than PMMA, the cost of such a process would be a strong deterrent for a non-high-mass production. It follows that if one cannot ensure the integrity of the bottom layer, there is the opportunity to use the ablation of a thin top layer to induce chemical and physical changes in the top surface of the bottom layer. With all this background, the principle of the fabrication of the microwells is presented in Figure 1.

Mapping Surface Hydrophobicity with AFM. AFM can be used not only for fine mapping of the topography of a surface but also for probing the physics and chemistry of the surface. In this context, AFM has been used to probe intermolecular interactions with pN sensitivity and spatial resolution of nanometers.[27] When there is imaging under ambient conditions, the capillary condensation between the tip and sample surfaces reflects the relative degree of hydrophilicity and can be used as a basis for discriminating between hydrophobic and hydrophilic groups.[28] The image contrast in a lateral force map is effectively a measure of tip-to-surface friction. Frictional force follows the generalized Amonton's law:[27,29,30]

$$F_f = \mu F_N + F_0 \quad (1)$$

Here μ is the friction coefficient, F_N is the lever-induced normal force, and F_0 is "residual force" which correlates with adhesion force between the tip and the sample surfaces.

Previous studies[27] have shown that the interaction forces between tips and samples which both terminate with hydrophobic groups are small. Observed interaction forces are also small when one of the surfaces terminates with hydrophobic groups and the other terminates with polar groups, whereas significant interactions are observed when both the tip and sample surfaces terminate with hydrophilic groups (hydrogen-bonding).

The Si_3N_4 tip used in our study is hydrophilic due to the native oxide surface layer. The frictional force is therefore higher as the tip is scanned across a hydrophilic surface, compared to a hydrophobic surface.

Microassays in a Microarray Format. Initially, we planned to approach the fabrication of the microassay in a classical microarray format. The results regarding this technical approach were mixed. Although the IgGs were successfully deposited in a succession of microablation and "blanket" incubation steps for several IgGs and control proteins, as presented in Figure 2, the deposition was not entirely reproducible with proteins having different apparent surface concentrations from microwell to microwell. Also it appears that the deposition of the protein is uneven, i.e., distribution of concentration transversal to the ablated lines. From here we inferred that the large variations in the local ablation energy induce important variations in the surface properties of the polymer beneath the ablatable layer, with important variations in the protein concentration.

To explore further the interactions among laser power−surface properties−protein adsorption, we ablated 50 × 50 μm areas at different ablation energies, as well as a few lines, and then we locally deposited and incubated fluorescently labeled antibody (anti-chiken IgG AlexaFluor 546; results in Figure 3). It appears that the proteins deposit primarily on the regions at the edges of the ablated areas and that, after a certain power threshold (around

(27) Noy, A.; Vezenov, D. V.; Lieber, C. M. *Annu. Rev. Mater. Sci.* **1997**, *27*, 381−421.
(28) Wilbur, J. L.; Biebuyck, H. A.; MacDonald, J. C.; Whitesides, G. M. *Langmuir* **1995**, *11*, 825−831.
(29) Sinniah, S. K.; Steel, A. B.; Miller, C. J.; Reutt-Robey, J. E. *J. Am. Chem. Soc.* **1996**, *118*, 8925−8931.
(30) Vezenov, D. V.; Noy, A.; Rozsnyai, L. F.; Lieber, C. M. *J. Am. Chem. Soc.* **1997**, *119*, 2006−2015.

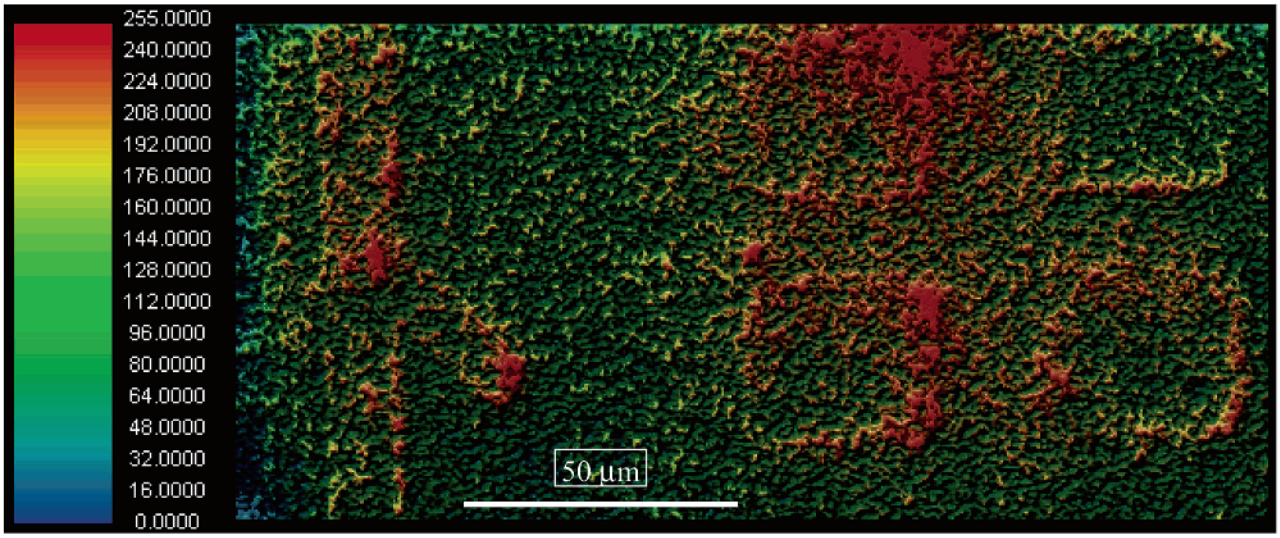

Figure 3. Fluorescence images of anti-chiken IgG AlexaFluor 546-conjugated deposited on the Au−PMMA bilayer exposed to different laser doses. The upper left area is ablated with 60% laser power with the bottom left 100%, upper right 40%, and bottom right 80%, respectively. The color scale on the left represents the intensity of the fluorescence of the adsorbed protein.

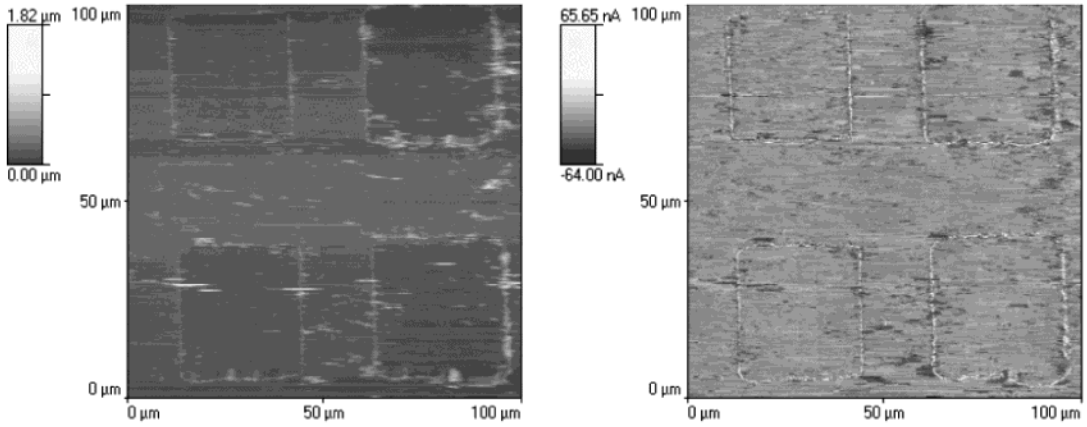

Figure 4. Topographical (left) and friction force (right) images of the Au−PMMA bilayer structure exposed to different laser doses. The upper left area is ablated with 40% laser power with the bottom left 60%, upper right 80%, and bottom right 100%, respectively.

50%), this concentration levels off. In principle, the higher concentration of the protein could be an artifact resulting from the verticality of the wall (apparently thicker protein layer seen from the top of a vertical wall). However, the height of the wall is not large (around 50 nm) and, more importantly, the AFM analysis (Figure 4) points out the real differences in the material characteristics near the edges of the ablated area. First, the lateral force measurements, taken before protein deposition, proves that the outer surface (Au) has a similar hydrophobicity with the inner area (PMMA) in line with the similar contact angles for these two materials (around 65 and 70°, respectively). Second, the AFM-measured topography shows that indeed the bottom of the well is deeper and rather flat, except for the edges that are elevated above the level of the gold layer. Third, the AFM mapping of the lateral force clearly shows a hydrophilic rim at the edges of the ablated area (areas in Figure 4, right side), possibly guarded by thinner hydrophobic stripe (brighter and darker areas in Figure 4, right, respectively). Moreover, the width of the rim seems to be rather independent of the laser power.

Bar Code Microassays. Because most of the protein is confined at the edges of the ablated areas, we concluded that the ablation of larger rectangular areas in the bilayer films as described above is a largely inefficient method for building microstructures for protein microassays. The logical approach is to fabricate linear microstructures which will both decrease the actual amount of protein used for deposition, especially if a spatially addressable deposition is used, as well as increase the capacity for miniaturization in a lateral if not in a 2D manner. The other benefit of this approach arises from the possibility to encode the information (e.g. type of antibody, concentration) through a combination of vertical lines in a "bar code", "informationally addressable" mode and not in a 2D, spatially addressable mode like in the classical microarrays. The results also demonstrate, inter alia, the complexities of protein adsorption in microfabricated channels, with the resolution of the variation of the protein concentration in the nanometer range. These complexities are likely to have an increasingly important impact in microfluidics, especially for devices that comprise nanochannels.

The AFM topography and lateral force imaging, as well as the knowledge regarding laser ablation, allow us to propose the following mechanism of formation of the observed microstructures and subsequent variations in protein adsorption. Laser exposure (ns) causes the overheating of PMMA to a point where the polymer is melted and chemical reactions start to occur. The expected reactions would be, in the order of increasing pyrolysis temperature, (i) the termination of the side ester groups at one of the C−O bonds, resulting in a more hydrophilic

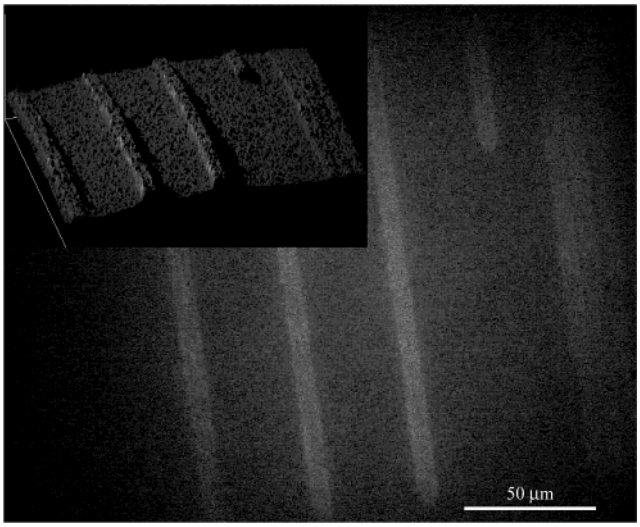

Figure 5. Fluorescence images of anti-chicken IgG AlexaFluor 546-conjugated deposited on the "bar code" microstructure fabricated in a Au−PMMA bilayer. From left to right, the 1st line shows the ablation with 100% of laser power at a rate of 20 pulse/s and the writing speed of 10 μm/s, the 2nd line shows ablation with 100% of laser power at a rate of 20 pulse/s and a writing speed of 10 μm/s, repeated twice, and the 3rd line shows ablation with 100% of laser power at a rate of 20 pulse/s and a writing speed of 20 μm/s. The inset represents a pseudomap of the intensity of the fluorescence.

material, (ii) depolymerization of the main chain, preserving the same hydrophobicity, and, if the process is quick enough, (iii) the breaking of the side bonds, resulting in a more hydrophobic material. Therefore, we can hypothesize that there are three regions in the microwell. At the center of the ablated line where the thermal energy would reach a maximum the decomposition is the most advanced, PMMA would experience the breaking side chain C−C groups, resulting in a more hydrophobic material. Between the center and the edge of the ablated line the polymer undergoes depolymerization only. At the edges of the line, where the thermal energy has the lowest levels and the remaining metal layer absorbs the overheating, the polymer is deesterified (with generation of gases), melted and expulsed over the edges of the microwell, resulting in a porous, more hydrophilic zone.

Proteins adsorb either via hydrophobic interactions between hydrophobic patches on the molecular surface and adsorbing surfaces or via weaker electrostatic interactions between charged patches and charged surfaces. It follows that the protein will be adsorbed at the center of the microwell and on the porous zone at the edges. On rectangular ablated areas, where the center of the microwell is ablated by subsequent sweeps of the laser beam, much of the protein adhesion occurs at the edges of the ablated area.

The processing conditions (e.g. laser power, speed of writing) were tested to clarify the optimal surface treatment that will facilitate the best and reproducible protein attachment. The results of this experiment are presented in Figure 5. Protein attachment reached a maximum on

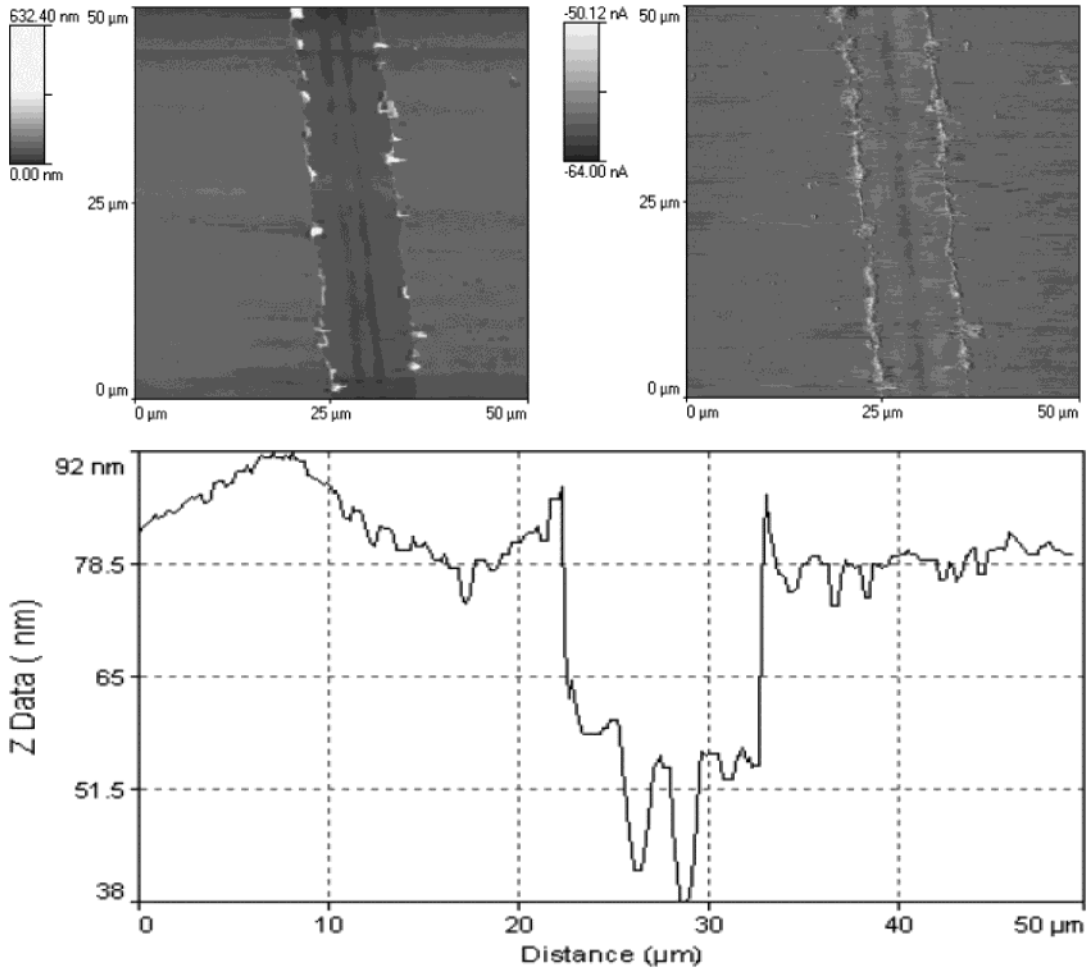

Figure 6. Topographical (top left) and friction force (top right) images of a channel created by the laser beam (100% laser power, 20 pulse/s, and 10 μm/s writing speed). The bottom plot represents the profile of a transversal section of the channel.

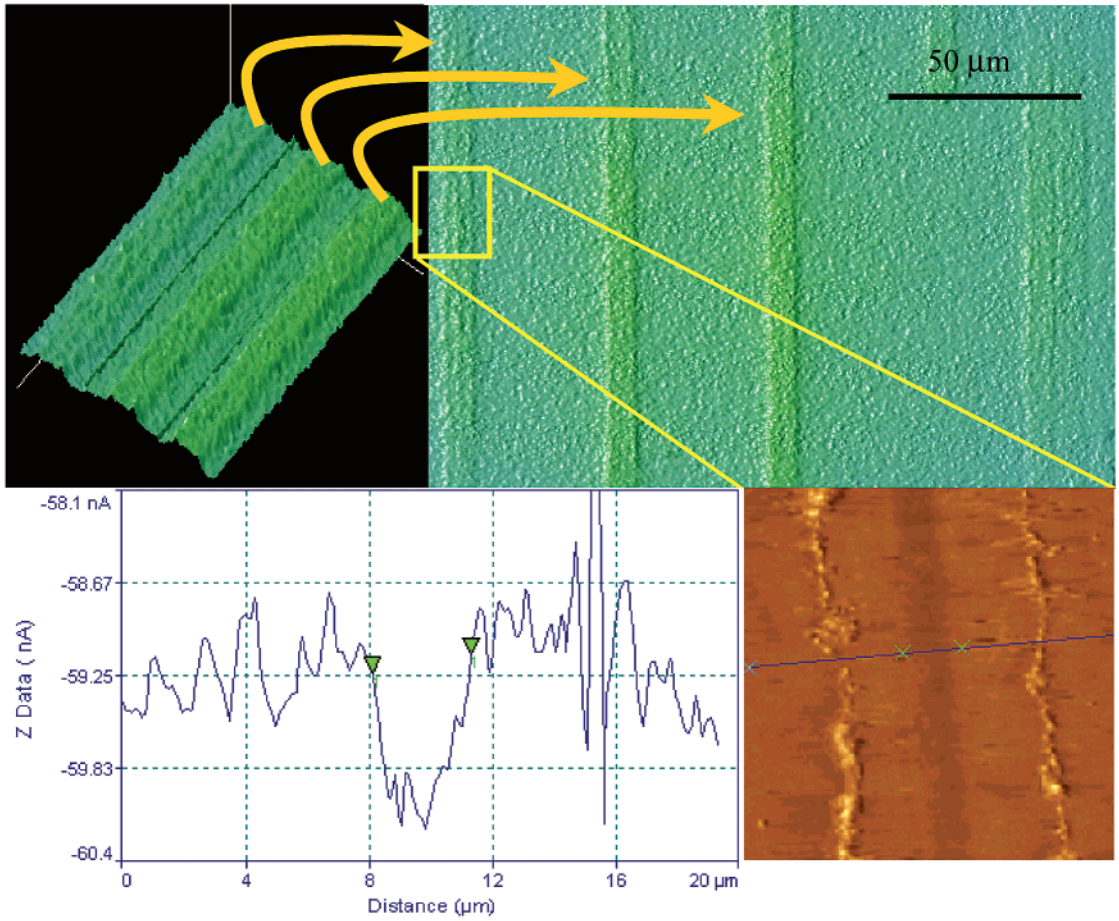

Figure 7. Fluorescence images of the labeled protein adsorbed on microstructures fabricated via laser ablation at different power levels (conditions as in Figure 6). The amplification of fluorescence (in inset on each line) and the pseudomap of the intensity of the fluorescence (inset upper left) compared with the hydrophobicity map (inset upper right) reveal a "fine structure" of protein deposition, preferentially on the hydrophilic edges of the channel and on the hydrophobic ridge on the center of the channel.

the lines ablated with 100% of the laser power and at the highest pulse rate (i.e. 20 pulse/s, line no. 3 from the left in Figure 5). When using the same total energy, but via the ablation with a rate of 10 pulse/s repeated twice (lines no. 1 and 2 from the left, respectively), the protein adsorption was less apparent. Therefore, further experiments used this optimized parameters for the microfabrication of the protein patterns.

To understand the protein adsorption in microablated channels and compare with the adsorption on rectangular features, we analyzed the inner surface of the channels using AFM (Figure 6). Apart from the hydrophilic elevated ridges observed before, the AFM analysis has revealed a hydrophobic elevation from the bottom of the channel line. The high-resolution images of the fluorescence compared with high-resolution AFM lateral force mapping (Figure 7) reveal a "fine structure" of protein deposition, preferentially on the hydrophilic edges of the channel and on the hydrophobic ridge on the center of the channel.

We infer that the high specific surface of the channel, which is caused by either the uneven bottom of the channel or by the possible porous material of the ridges, cooperates with the many variations of the surface hydrophobicity to allow a high concentration of diverse proteins in the microablated channels compared with rectangular ablated areas.

Specific Antibodies Recognition. The protein detection system described above was demonstrated by the incubation of the bar code microassay (fabricated as described above) with both IgG's and control proteins. For an example, Figure 8 presents a part of a microarray format with a bar code microstructure that was functionalized with two proteins, before (top image, bright field) and after protein recognition (bottom image, fluorescence). Chicken IgG was deposited on a fragment of the bar code microstructure (three lines on the right, Figure 8, top) and streptavidin was deposited on the rest of the microstructure (two lines on the left, Figure 8, top) using the picoliter pipet. The anti-chicken IgG deposited over the whole microarray of specifically recognized the chicken IgG lines (bottom image).

Conclusions

A novel method for the fabrication of microstructures via the selective ablation of an ablatable thin layer (such as 50 nm gold) deposited on top of a polymeric surface that promotes protein adsorption (such as poly(methyl methacrylate) is presented. This method was used for the fabrication of protein microassays in a microarray format. As the adsorbed protein is mainly confined at the edges of the ablated areas, the ablation of larger rectangular areas is a largely inefficient method. Linear microstructures both decrease the actual amount of protein used for deposition, especially if a spatially addressable deposition is used, and increase the capacity for miniaturization in a lateral non-2D manner. Also this approach opens the possibility to encode the information (e.g. type of antibody, concentration) through a combination of vertical lines in a "bar code", "informationally addressable" mode and not

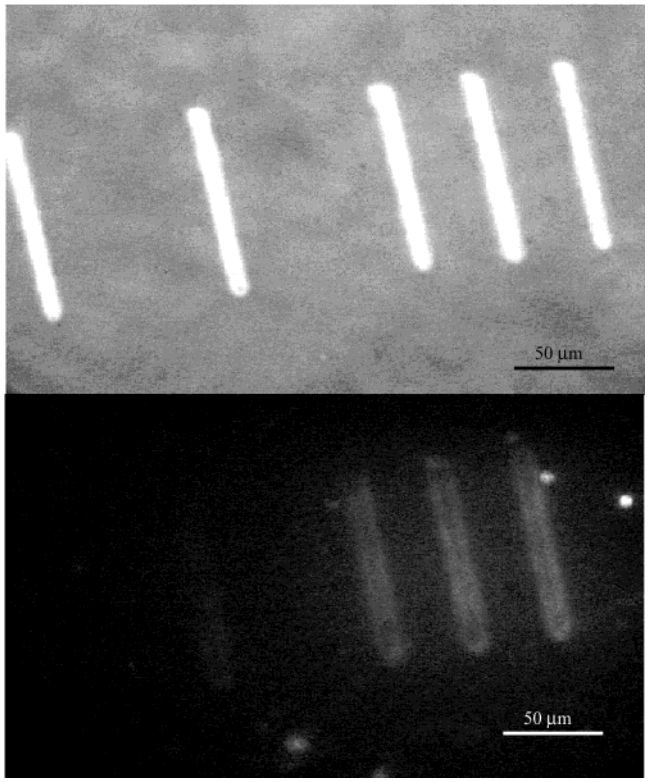

Figure 8. Detection of specific antigens in high-density "bar code" array format demonstrated by incubation of the array with fluorescently labeled individual or collective antibodies. On the top is a fragment of bar code array of two different proteins in the bright field; on the bottom, a fluorescent image of the same array with specific recognition by anti-chicken IgG AlexaFluor 546 conjugate.

in a 2D, spatially addressable mode like in the classical microarrays.

Experimental Section

Protein Preparations. Several immunoglobulins (IgG's), i.e., bovine IgG, chicken IgG, human IgG, rabbit IgG, and affinity isolated antigen-specific corresponding antibodies (whole molecule), were purchased from Sigma. Streptavidin and fibrinogen were used as control proteins. The IgGs were prepared as stock solutions at a concentration of 2 mg/mL and diluted with PBS to 100 μg/mL as working solutions prior to experiments.

Three fluorescent labels have been used, namely, fluorescein isothioiocyanate (FITC), AlexaFluor 456, and AlexaFluor 350. The FITC and AlexaFluor fluorescent tags have been conjugated to the selected proteins using FluoroTag Kits purchased from Sigma and Molecular Probes, respectively. The labeling procedure was carried out according to the instructions of the manufacturer. Each protein was used in concentration of 2 mg/mL. The labeled proteins were purified from unconjugated fluorescent dyes using a Sephadex G-25 column. The concentration of antigen conjugate was determined by UV−vis spectroscopy. The fluorescent dye/protein molar ratio of the purified protein was determined by measuring the absorbance at 280 nm (for protein), 495 nm (for FITC), 556 nm (for AlexaFluor 546), and 346 nm (for AlexaFluor 350).

Preparation of the Microfabricated Structures. Glass slides or cover slips (0.17 mm thick, 24 × 24 mm, Knittel) were sonicated in Nanopure water for 30 min and washed copiously with filtered (0.2 μm) Nanopure water (18.2 MΩ/cm), dried under a stream of high-purity nitrogen, and then primed with hexamethyldisilazane. A 4 wt % solution of PMMA in 99% propylene glycol methyl ether acetate (PGMEA) (purchased from Sigma Aldrich Co.) was spin-coated at 3000 rpm for 40 s using a Specialty Coating Systems spin coater (model P6708). For these conditions, the PMMA film thickness was 0.5 μm. The coated substrates were then soft baked at 85 °C for 30 min and stored in a desiccator prior to and after gold deposition. The deposition of gold was done using a sputtering SEM-coating unit E5100 (Polaron Equipment Ltd.) at 25 mA for 90 s at 0.1 Torr. For these conditions, the gold film thickness was 50 nm. The gold-layered substrata were then incubated with bovine serum albumin (BSA) by immersion in a 1% w/v BSA 10 mM phosphate-buffered saline (PBS) solution (pH 7.4) at room temperature for approximately 1 h and then rinsed with PBS followed by Nanopure water.

The laser-based microfabrication of gold-coated polymeric films can be readily accomplished with commercially available microscope adaptations. The system (Cell Robotics, Inc.) comprised a Nikon Eclipse TE300 inverted microscope, coupled with a computer-controlled, pulsed nitrogen laser emitting at 337 nm with a maximum intensity of 120 μJ/pulse and focused directly through the microscope objective lens.

Quantification of Surface-Related Processes. The hydrophobicity of the films was estimated by contact-angle measurements. Advancing contact angles were measured on sessile drops (2 μL) of Nanopure water at room temperature (20−23 °C) in air using a contact angle meter constructed from an XY stage fitted with a (20 μL) microsyringe, a 20× magnification microscope (ISCO-OPTIC, Gottingen, Germany), and a fiber-optic illuminator. The observed values were averaged over six different readings.

Atomic force microscopy (AFM) was carried out on an Explorer system (ThermoMicroscopes) in the normal contact mode. The AFM system is based on detection of tip-to-surface forces through monitoring optical deflection of a laser beam incident on a force-sensing/imposing lever. Several scanners were used in order to cover the scales of lateral topographical and chemical differentiation; the fields-of-view ranged from 100 × 100 μm down to 8 × 8 μm. The analyses were carried out under air-ambient conditions (temperature of 23 °C and 45% relative humidity). Pyramidal-tipped, silicon nitride cantilevers with a spring constant of 0.032 N/m were used. As the tip is scanned across the surface, the lateral force acting on the tip manifests itself through a torsional deformation of the lever, which is sensed by the difference signal on the left−right signal on the quadrant detector. The difference signal can be plotted as a function of XY location in the topographical field of view, and the resulted friction force image can then be correlated directly with the topographical image. In this study, the lateral force imaging was performed simultaneously with topographical imaging in both forward and reverse scan directions.

The attachment of fluorescently labeled proteins on the ablated microstructures was visualized and analyzed using two different microscopic systems. The first is a Nikon TE300 inverted microscope, coupled with an epi-fluorescence illumination unit fitted with filter sets specific toward FITC (CR101, Chroma Technology) and AlexaFluor (XF108-2, Omega Optical, Inc.). The second was a Nikon Microphot FX microscope with a UV light source (Nikon Mercury Lamp, HBO-100 W/2; Nikon C.SHG1 super-high-pressure mercury lamp power supply) at 100× objective. These images were captured on a Nikon camera (FX-35WA). The fluorescent images were observed using an intensified CCD video camera, Lumi Imager (Photonic Science), and processed using PaintShop Pro (Jasc Software). The fluorescence intensities were analyzed using Gel-Pro Analyzer software, version 4.0.

Multianalyte Antibody Microassay. The microassays fabricated as described above comprised different IgGs (1−7 μL of 100 μg/mL), either fluorescently labeled for the visualization of the selectivity of protein attachment or unlabeled for the visualization of the selectivity of protein recognition by labeled antigens, deposited onto micropatterned ablated areas as described above.

For microassay fabrication and process monitoring and optimization, IgG conjugates with FITC and AlexaFluor's (2−7 μL of 100 μg/mL) were deposited onto microfabricated ablated geometries either in a "blanket" mode, flooding the whole surface of the microassay, or in a spatially addressable manner, using the picoliter pipet. For the blanket deposition, the slide was incubated for 30 min at room temperature in a humid chamber and then the slide was washed three times with PBS and twice with Nanopure water. The spatially addressable deposition used

a picoliter pipet (CellSelector module, Cell Robotics Inc.) mounted on the same precision XY stage. Very small amounts, usually around few hundreds of nanoliters down to hundreds of picoliters, can be deposited in precise locations, usually within micrometer-range precision.

For the testing of the microassays, the IgGs-covered surfaces were incubated individually or collectively with corresponding fluorescently labeled antibodies and control proteins (e.g. fibrinogen, streptavidin) for 2 h at room temperature. The microassays structures were then washed three times with PBS and twice with Nanopure water. The images of the selectively recognized micropatterned features were analyzed as described above.

Acknowledgment. This study was sponsored by the Defence Advanced Research Projects Agency (DARPA) Grant No. N66001-00-18952. E.P.I. and L.F. also acknowledge the partial support from a Science Support Foundation (RAS) grant for talented researchers and the postgraduate scholarship from CRC for Microtechnology, respectively.

LA0260178